American Mineralogist, Volume 102, pages 357–368, 2017

Equation of state and hyperfine parameters of high-spin bridgmanite in the Earth's lower mantle by synchrotron X-ray diffraction and Mössbauer spectroscopy

Zhu Mao[1,*], Fan Wang[1], Jung-Fu Lin[2,3,*], Suyu Fu[1,2], Jing Yang[2], Xiang Wu[4], Takuo Okuchi[5], Naotaka Tomioka[6], Vitali B. Prakapenka[7], Yuming Xiao[8], and Paul Chow[8]

[1]Laboratory of Seismology and Physics of Earth's Interior, School of Earth and Planetary Sciences, University of Science and Technology of China, Hefei, Anhui 230026, China
[2]Department of Geological Sciences, Jackson School of Geosciences, The University of Texas at Austin, Austin, Texas 78712, U.S.A.
[3]Center for High Pressure Science and Technology Advanced Research (HPSTAR), Shanghai 130012, China
[4]State Key Laboratory of Geological Processes and Mineral Resources, China University of Geosciences, Wuhan 430074, China
[5]Institute for Study of the Earth's Interior, Okayama University, Misasa, Tottori 682-0193, Japan
[6]Kochi Institute for Core Sample Research, Japan Agency for Marine-Earth Science and Technology, Nankoku, Kochi 783-8502, Japan
[7]Center for Advanced Radiation Sources, University of Chicago, Chicago, Illinois 60637, U.S.A.
[8]HPCAT, Geophysical Laboratory, Carnegie Institution of Washington, Argonne, Illinois 60439, U.S.A.

Abstract

In this study, we performed synchrotron X-ray diffraction (XRD) and Mössbauer spectroscopy (SMS) measurements on two single-crystal bridgmanite samples [$Mg_{0.94}Fe^{2+}_{0.04}Fe^{3+}_{0.02}Al_{0.01}Si_{0.99}O_3$ (Bm6) and $Mg_{0.89}Fe^{2+}_{0.024}Fe^{3+}_{0.096}Al_{0.11}Si_{0.89}O_3$ (Al-Bm11)] to investigate the combined effect of Fe and Al on the hyperfine parameters, lattice parameters, and equation of state (EoS) of bridgmanite up to 130 GPa. Our SMS results show that Fe^{2+} and Fe^{3+} in Bm6 and Al-Bm11 are predominantly located in the large pseudo-dodecahedral sites (A-site) at lower-mantle pressures. The observed drastic increase in the hyperfine quadrupole splitting (QS) between 13 and 32 GPa can be associated with an enhanced local distortion of the A-site Fe^{2+} in Bm6. In contrast to Bm6, the enhanced lattice distortion and the presence of extremely high QS values of Fe^{2+} are not observed in Al-Bm11 at high pressures. Our results here support the notion that the occurrence of the extremely high QS component of approximately 4 mm/s in bridgmanite is due to the lattice distortion in the high-spin (HS) A-site Fe^{2+}, instead of the occurrence of the intermediate-spin state. Both A-site Fe^{2+} and Fe^{3+} in Bm6 and Al-Bm11 remain in the HS state at lower-mantle pressures. Together with XRD results, we present the first experimental evidence that the enhanced lattice distortion of A-site Fe^{2+} does not cause any detectable variation in the EoS parameters, but is associated with anomalous variations in the bond length, tilting angle, and shear strain in the octahedra of Bm6. Analysis of the obtained EoS parameters of bridgmanite at lower-mantle pressures indicates that the substitution of Fe in bridgmanite will cause an enhanced density and a reduced bulk sound velocity (V_Φ), whereas the Al and Fe substitution has a reduced effect on density and a negligible effect on V_Φ. These experimental results provide new insight into the correlation between lattice, hyperfine, and EoS parameters of bridgmanite in the Earth's lower mantle.

Keywords: Bridgmanite, lattice distortion, equation of state, Fe and Al, lower mantle, high spin

Introduction

Bridgmanite, $(Mg,Fe)(Fe,Al,Si)O_3$, is the most abundant mineral in the Earth's lower mantle occupying approximately 75% by volume in a pyrolitic mantle composition or as high as ~93% in the chondritic Earth model with a Si-enriched lower mantle (Hirose 2002; Irifune et al. 2010; Murakami et al. 2012; Ringwood 1975). In the past few decades, physical properties of bridgmanite at relevant pressure and temperature (*P*-*T*) conditions of the lower mantle have attracted extensive research interest (e.g., Hemley and Cohen 1992; McCammon 1997; Stixrude and Cohen 1993; Tsuchiya et al. 2004). In particular, recent experimental and theoretical studies have reported that Fe in lower-mantle bridgmanite undergoes spin pairing transitions, calling for investigations into the effect of Fe spin transition on the physical properties of bridgmanite at lower-mantle pressures (e.g., Catalli et al. 2011, 2010; Goncharov et al. 2010; Hsu et al. 2012; Lin et al. 2008, 2012; Mao et al. 2011, 2015; McCammon et al. 2008; Tsuchiya and Wang 2013). However, the spin and valence states of iron in bridgmanite remain controversial (e.g., see Lin et al. 2013 for a review).

Fe can exist as both Fe^{2+} and Fe^{3+} in lower-mantle bridgmanite in large pseudo-dodecahedral sites (A site) and small octahedral sites (B site) (Lin et al. 2013), complicating our understanding of the spin states of Fe in bridgmanite. Thus far, both experimental and theoretical studies are in agreement that Fe^{3+} in the B site will undergo the high-spin (HS) to low-spin (LS) transition at lower-mantle pressures, but the A-site Fe^{3+} will stay in the HS

* E-mail: zhumao@ustc.edu.cn and afu@jsg.utexas.edu

state (Bengtson et al. 2009; Catalli et al. 2011, 2010; Dorfman et al. 2015; Fujino et al. 2014, 2012; Hsu et al. 2011, 2012; Lin et al. 2013, 2016). Although Fe^{2+} will only locate at the A site in bridgmanite, the spin state of Fe^{2+} is still under debate (Bengtson et al. 2009; Hsu et al. 2010; Hsu and Wentzcovitch 2014; Jackson et al. 2005; Li et al. 2006; Lin et al. 2012; McCammon et al. 2010, 2008; Shukla et al. 2015). High-pressure Mössbauer spectroscopy studies have shown that the quadrupole splitting (QS) of the A-site Fe^{2+} increases drastically to an extremely high value of ~4 mm/s at approximately 18–30 GPa (Lin et al. 2012, 2013; Mao et al. 2011; McCammon et al. 2010, 2008; Narygina et al. 2010). The anomalous increase in the QS of A-site Fe^{2+} in bridgmanite has been interpreted as the HS to intermediate-spin (IS) transition by high-pressure Mössbauer studies, which has been proposed to produce a softening in the spontaneous shear strain and affect the octahedral tilting during compression (Boffa Ballaran et al. 2012; Lin et al. 2008; McCammon et al. 2010, 2008; Narygina et al. 2010). However, theoretical calculations have pointed out that the IS Fe^{2+} in bridgmanite is energetically disfavored and highly unlikely to be stable at lower-mantle pressures, and the observed extremely high QS component is caused by the enhanced lattice distortion of the HS Fe^{2+} in the A site (Bengtson et al. 2009; Hsu et al. 2010; Hsu and Wentzcovitch 2014).

The influence of the spin states of Fe^{3+} and Fe^{2+} on the physical properties, in particular the equation of state (EoS), of bridgmanite is a crucial issue to understand the chemistry and dynamics of the lower mantle. Theoretical and experimental studies have shown that the spin transition of B-site Fe^{3+} in bridgmanite can cause an abrupt reduction in its unit-cell volume and softening in its bulk modulus at high pressure (Catalli et al. 2011; Hsu et al. 2011; Tsuchiya and Wang 2013). A recent experimental study has observed an anomalous collapse in the volume of bridgmanite with 10% Fe between 18 and 25 GPa at 300 K (Mao et al. 2015). The cause for the observed anomalous change in the volume of bridgmanite remains unclear because the spin transition of B-site Fe^{3+} occurs coincidently with the enhanced lattice distortion of A-site Fe^{2+}, and we still lack of direct experimental evidence for the effect of enhanced lattice distortion of A-site Fe^{2+} on the EoS parameters of bridgmanite (Mao et al. 2015). In addition, most previous high-pressure studies for the EoS of bridgmanite did not determine the spin and valence states of Fe in the powder samples at high pressures, complicating our understanding of the effects of different spin and valence states of Fe on the EoS of bridgmanite (Andrault et al. 2001; Boffa Ballaran et al. 2012; Dorfman et al. 2013; Lundin et al. 2008; Mao et al. 1991; Nishio-Hamane et al. 2008).

Besides Fe, lower-mantle bridgmanite is expected to accommodate ~10% Al via the coupled substitution of Fe^{3+}-Al^{3+} and/or Al^{3+}-Al^{3+} to replace Mg^{2+} in the pseudo-dodecahedral A site and the octahedral B-site Si^{4+} (Frost et al. 2004; Irifune et al. 1996, 2010; McCammon 1997; Vanpeteghem et al. 2006). The Fe^{2+}, Fe^{3+}, and Al^{3+} contents in bridgmanite in a pyrolitic composition have been reported to change with depth in the lower mantle (e.g., Irifune et al. 2010). Theoretical calculations have shown that the addition of Al does not affect the response of the A-site Fe^{3+} spin states to pressure (Hsu et al. 2012), yet how the presence of Al may influence the lattice distortion of A-site Fe^{2+} is unknown. In addition, although previous experimental studies have yielded a wealth of results on the effects of Fe and Al on the EoS parameters of bridgmanite using X-ray diffraction (XRD) in a diamond-anvil cell (DAC), the spin states of Fe in (Fe,Al)-bearing bridgmanite are mostly not determined in these studies, and the experimental results on the combined effects of Fe and Al on the EoS parameters of bridgmanite are still controversial (Andrault et al. 2001; Boffa Ballaran et al. 2012; Dorfman et al. 2012; Glazyrin et al. 2014; Nishio-Hamane et al. 2008). For example, Andrault et al. (2001) showed that the presence of Fe and Al can increase the isothermal bulk modulus at ambient conditions, K_{0T}, by 4% relative to that of $MgSiO_3$-bridgmanite (Mg-Bm) if the initial pressure derivative of the isothermal bulk modulus, K'_{0T}, is fixed to the value of 4. In contrast, two other studies have shown that the presence of 11–13% Fe and 12–15% Al leads to a 3–4% reduction in K_{0T} with a fixed $K'_0 = 4$ using Mg-Bm as the reference (Catalli et al. 2011; Nishio-Hamane et al. 2008). As a result, the effects of the Al and Fe chemistry variation and iron valence and spin state on the derived EoS parameters of these bridgmanite samples remain poorly understood.

To correlate the lattice parameters with the hyperfine parameters (spin and valence states) of iron in bridgmanite and to better constrain the effect of Fe and Al on its density and sound velocity in the lower mantle, direct examinations of the hyperfine, lattice, and EoS parameters of high-quality Fe-bearing and (Fe,Al)-bearing single-crystal bridgmanite with well-characterized iron valence states, site occupancy, spin states, and crystal chemistry are needed to provide new insights into these aforementioned outstanding issues. In this study, we have performed high-pressure synchrotron XRD and SMS measurements on two single-crystal bridgmanite samples ($Mg_{0.95}Fe_{0.06}Si_{0.99}O_3$ and $Mg_{0.89}Fe_{0.12}Al_{0.11}Si_{0.89}O_3$) up to 130 GPa and 300 K. SMS is used as a unique probe to determine hyperfine parameters and to infer the spin and valence states of Fe in the single-crystal samples at lower-mantle pressures, while analysis of high quality single-crystal XRD data reveals local lattice parameters and bulk compression of bridgmanite crystals at high pressures. These results allowed us to correlate the occurrence of the extremely high quadrupole splitting of Fe^{2+} with the A-site local lattice distortion in the high-spin state and to model the effects of Fe and Al on the density and bulk sound velocity profiles of bridgmanite at lower-mantle pressures.

Experimental details

We synthesized single-crystal bridgmanite samples using the 5000-ton Kawai-type multi-anvil apparatus at Okayama University at Misasa, Japan (Okuchi et al. 2015). Fe-bearing bridgmanite with run number 5k2174 was synthesized using a mixture of ground $MgSiO_3$, $Mg(OH)_2$, and ^{57}FeO in an appropriate ratio as the starting sample, while the (Fe,Al)-bridgmanite with run number 5k2179 was synthesized using a mixture of ground $MgSiO_3$, $Mg(OH)_2$, Al_2O_3, and ^{57}FeO (Okuchi et al. 2015). Here, ^{57}Fe-enriched FeO (>95% enrichment) was used in the synthesis to enable high-pressure Mössbauer spectroscopy measurements in a DAC. Each starting mixture was cold-sealed into a Pt capsule, and compressed to 24 GPa. At this pressure, the material was heated at 1650 °C for 5.5 h for run 5k2174 and at 1750 ° C for 7 h for run 5k2179. For each run, the synthesis temperature was determined from the power-temperature relation of the cell assemblage that was calibrated using a W97Re3/W97Re25 thermocouple. The obtained single crystals were examined by an electron microprobe to confirm their chemical compositions and homogeneity, showing a homogeneous composition of $Mg_{0.94}Fe_{0.06}Al_{0.01}Si_{0.99}O_3$ (Bm6) in run 5k2174 and $Mg_{0.89}Fe_{0.12}Al_{0.11}Si_{0.89}O_3$ (Al-Bm11) in run 5k2179 (Okuchi et al. 2015). Considering the measurement error of the electron microprobe to be 1% and the low concentration of Al_2O_3 in Bm6, the Bm6 sample can be considered as an Al-

free bridgmanite. Single-crystal XRD measurements performed at 1 bar and 300 K proved that the synthesized single crystals in both compositions were in the silicate perovskite structure (*Pbnm*). The refined cell parameters are: a = 4.7880(2) Å, b = 4.9339(2) Å, c = 6.8983(3) Å for Bm6 and a = 4.7867(2) Å, b = 4.9569(2) Å, c = 6.9141(4) Å for Al-Bm11 at ambient conditions. The full-width at half maximum (FWHM) for each diffraction peak of each given crystal is ~0.044°, indicating that the synthesized single crystals are of a high quality.

These crystals were also analyzed using conventional Mössbauer spectroscopy at ambient conditions to determine the hyperfine parameters and to refer the spin and valence states of Fe in the samples. Mössbauer spectra, accumulated for 3 days for each composition, were recorded at room temperature in transmission mode on a constant acceleration Mössbauer spectrometer with a nominal 370 MBq ^{57}Co high specific activity source in a 12 μm thick Rh matrix. The velocity scale was calibrated relative to a 25 μm thick α-Fe foil using the positions certified for (former) National Bureau of Standards standard reference material no. 1541. The conventional Mössbauer spectra were fitted using the program MossA to Lorentzian doublets according to current models in the literature, and the usual constraints were applied to all doublets (equal component areas and widths) (Lin et al. 2016; Prescher et al. 2012).

For SMS measurements, we selected Bm6 and Al-Bm11 crystals less than 25 μm thick that were polished using a 3M diamond film and water as lubricant. The use of water during polishing was intended to prevent potential heating up and amorphisation. A sample platelet for each composition approximately 10 μm thick and 40 μm wide was loaded into a symmetric DAC equipped with a pair of beveled diamonds with 150/300 μm culet. NaCl was used as the pressure medium. The fluorescence shift of the ruby R_1 peak was used for the pressure calibration when the pressure was less than 80 GPa (Mao et al. 1986). Above 80 GPa, the ruby fluorescence peak was too broad and weak to be a reliable calibrant. We thus used the edge of the first-order Raman peak measured from one of the diamond anvils for the pressure calibration above 80 GPa (Akahama and Kawamura 2006). The SMS measurements were conducted at High Pressure Collaborative Access Team (HPCAT) of the Advanced Photon Source (APS), Argonne National Laboratory (ANL). An incident X-ray beam with an energy of 14.4125 keV and a bandwidth of 2 meV was used to excite the ^{57}Fe nuclei in the sample. An avalanche photodiode detector (APD) was used to collect the SMS signals with a typical collection time of ~4 to 6 h for each spectrum. Mössbauer spectra of the sample were collected with and without a stainless steel foil (~10 μm thick) with natural ^{57}Fe abundance at each given pressure in pressure steps of ~7 to 8 GPa up to 85 GPa for Bm6 and up to 130 GPa for Al-Bm11. The stainless steel foil was placed in front of the sample and used as a reference to determine the chemical shift of the Fe sites.

High-pressure XRD experiments of the single-crystal samples were carried out at GeoSoilEnviroCARS (GSECARS) of the APS, ANL. We used the same batch of the single crystals of Bm6 and Al-Bm11 as in the SMS experiments. The single-crystal samples were polished down to ~5 μm in thickness and loaded into sample chambers drilled in Re gaskets in DACs equipped with a pair of beveled diamonds with 150/300 μm culet. Pt powder slightly packed to ~5 μm thick was placed next to the single-crystal bridgmanite sample to determine the pressure, while He was used as the pressure medium in the sample chamber. In total, we made two runs of XRD measurements for each composition at room temperature. Diffraction patterns of bridgmanite single crystals were collected by rotating ±15° about the vertical axis of the sample stage to allow collecting as many diffraction spots as possible. The pressure step for the measurements was ~1 to 2 GPa.

Results

The analysis of the obtained conventional Mössbauer spectra showed that 45% of the total Fe in Bm6 is Fe^{3+} with QS = 0.32 mm/s and CS = 0.24 mm/s, while the remaining 55% Fe is in Fe^{2+} with QS = 1.63 mm/s and CS = 1.16 mm/s. Fe in Al-Bm11 is dominated by 80% Fe^{3+} with QS = 0.92 mm/s and CS = 0.46 mm/s. Only 20% Fe in Al-Bm11 is Fe^{2+} with QS = 1.79 mm/s and CS = 1.20 mm/s.

The obtained SMS spectra of Bm6 between 1 and 13 GPa are characterized by two time beats (Fig. 1). It should be noted that the spectra of Bm6 start to change greatly from 13 to 32 GPa with more time beats observed. Above 32 GPa and up to 85 GPa, 4 time beats were observed for Bm6, indicating the presence of a high quadrupole splitting (QS) component in the sample. In contrast to Bm6, the SMS spectra of Al-Bm11 only exhibit a slight change

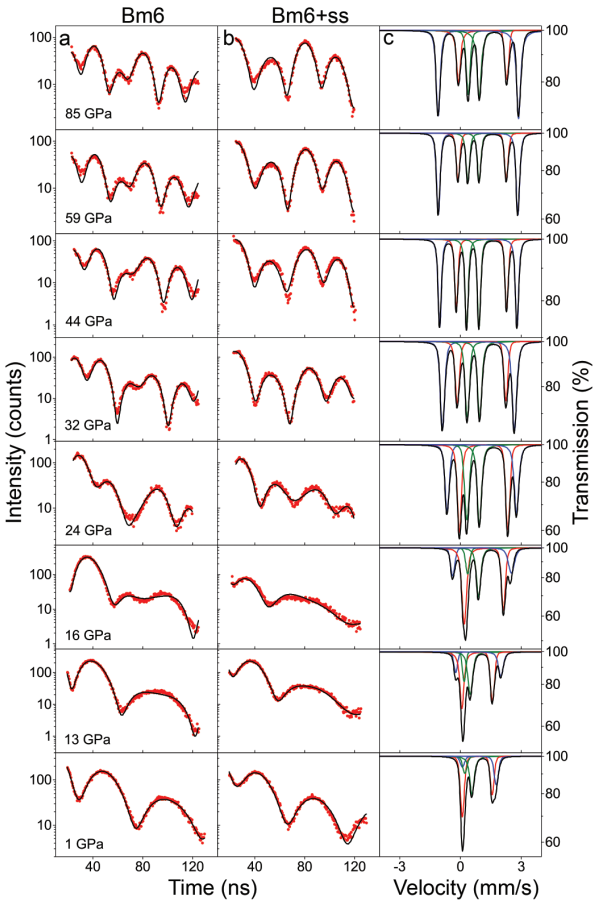

Figure 1. Representative synchrotron Mössbauer spectra and modeled energy spectra of Bm6 at high pressures and 300 K. Red circles = experimental spectra; black lines = modeled spectra using CONUSS program (Sturhahn 2000). Left panel = sample spectra; middle panel = spectra of sample plus stainless steel; right panel = energy spectra calculated from the fits in the left panel; blue line = doublet 1; red line = doublet 2; green line = doublet 3. (Color online.)

with increasing pressure up to 130 GPa (Fig. 2). Below 29 GPa, there is only a broad time beat observed in the SMS spectra of Al-Bm11, whereas the spectra change to exhibit two broad time beats between 29 and 130 GPa.

The Mössbauer spectra of both Bm6 and Al-Bm11 were analyzed using the CONUSS program to derive the hyperfine parameters and doublet abundances at high pressures (Figs. 1 and 2) (Sturhahn 2000). The SMS spectra for Bm6 can be well represented using a three-doublet model (Fig. 3). According to our derived QS and chemical shift (CS) values at 1 bar and literature results at ambient conditions, doublet 1 with QS = 1.63 mm/s and doublet 2 with QS = 1.50 mm/s at ambient conditions were assigned to be the HS Fe^{2+} in the A site, whereas doublet 3 with an extremely low QS value of 0.44 mm/s was assigned to be the HS Fe^{3+} in the A-site (Supplemental[1] Table S1) (Dyar et al. 2006).

[1]Deposit item AM-17-25770, Supplemental Material. Deposit items are free to all readers and found on the MSA web site, via the specific issue's Table of Contents (go to http://www.minsocam.org/MSA/AmMin/TOC/2017/Feb2017_data/Feb2017_data.html).

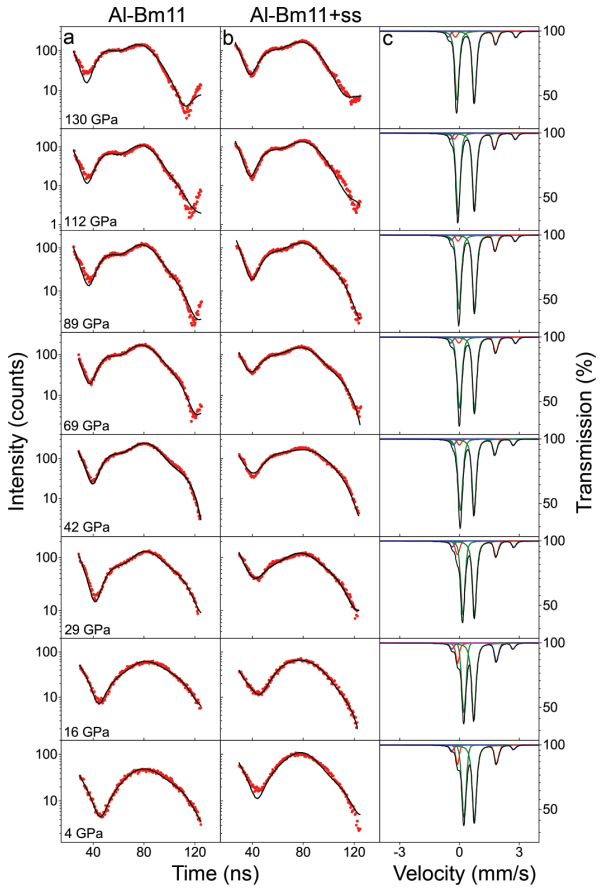

FIGURE 2. Representative synchrotron Mössbauer spectra and modeled energy spectra of Al-Bm11 at high pressures and 300 K. Red circles = experimental spectra; black lines = modeled spectra using CONUSS program (Sturhahn 2000). Left panel = sample spectra; middle panel = spectra of sample plus stainless steel; right panel = modeled energy spectra with assigned doublets calculated from the fits in the left panel. Blue = doublet 1; red = doublet 2; green = doublet 3. (Color online.)

A-site Fe^{2+} accounts for 66% of the total Fe in Bm6, which is in general agreement with the conventional Mössbauer results at ambient conditions. Combining the Mössbauer and electron microprobe results, the chemical formula for Bm6 is $Mg_{0.94}Fe^{2+}_{0.04}Fe^{3+}_{0.02}Al_{0.01}Si_{0.99}O_3$. We have kept the abundances of Fe^{2+} and Fe^{3+} constant for high-pressure spectral modeling. With increasing pressure, QS of doublet 1 exhibits a dramatic increase to 3.6 mm/s between 13 and 32 GPa and only a slightly increase with pressure to 4 mm/s up to 85 GPa. Although QS of doublet 2 for Bm6 also exhibits an abrupt increase between 13 GPa and 32 GPa, the variation of QS for doublet 2 with increasing pressure is much less than doublet 1. The abundance of doublet 2 significantly decreases with pressure between 13 and 32 GPa and is accompanied by an increase in the abundance of doublet 1, with a higher QS component at high pressures.

A three-doublet model was also used to fit the SMS spectra of Al-Bm11 (Fig. 3). Doublet 1 with QS = 2.90 mm/s and doublet 2 with QS = 1.69 mm/s at 4 GPa were assigned to be the HS Fe^{2+} in the A site, whereas doublet 3 with QS = 0.66 mm/s was assigned to be the HS Fe^{3+} based on literature results (Supplemental[1] Table S1) (Dyar et al. 2006). The total abundance of A-site Fe^{2+} is ~20%, which is consistent with the conventional Mössbauer results and does not change with increasing pressure. The chemical formula for Al-Bm11 can thus be written as $Mg_{0.89}Fe^{2+}_{0.024}Fe^{3+}_{0.096}Al_{0.11}Si_{0.89}O_3$ by combining the Mössbauer and electron microprobe results. For both doublets 1 and 2, their QS values show a weak increase with pressure, and the total abundance of doublet 1 and doublet 2 remains constant with increasing pressure. The conversion from the lower QS component to the higher QS component shown in Bm6 is not observed in Al-Bm11 (Fig. 3). Previous experimental studies have shown that addition of Al can cause an apparent increase in the volume of bridgmanite (Andrault et al. 2001; Boffa Ballaran et al. 2012). We speculate that the presence of Al also decreases the difference in volume between the sites hosting Fe^{2+} with high QS (doublet 1) and those hosting Fe^{2+} with low QS (doublet 2). As a result, the enthalpy of doublet 2 in our Al-Bm11 could be smaller than that of doublet 1 in the entire lower-mantle pressure range. The conversion from the low-QS doublet 2 to the high QS doublet 1 thus does not occur in Al-Bm11. In addition, QS of doublet 3 only exhibits a weak increase with pressure up to 130 GPa.

Single-crystal XRD patterns were collected from ambient conditions to pressures of 85 GPa for Bm6 and 110 GPa for Al-Bm11 at 300 K. The FWHM for each peak in our collected XRD patterns slightly increases from 0.044° at ambient conditions to ~0.059° at the maximum experimental pressure (Supplemental[1] Fig. S2), indicating the collected single-crystal XRD patterns are of a high crystal quality in a quasi-hydrostatic helium pressure medium. The obtained unit-cell volumes of both Bm6 and

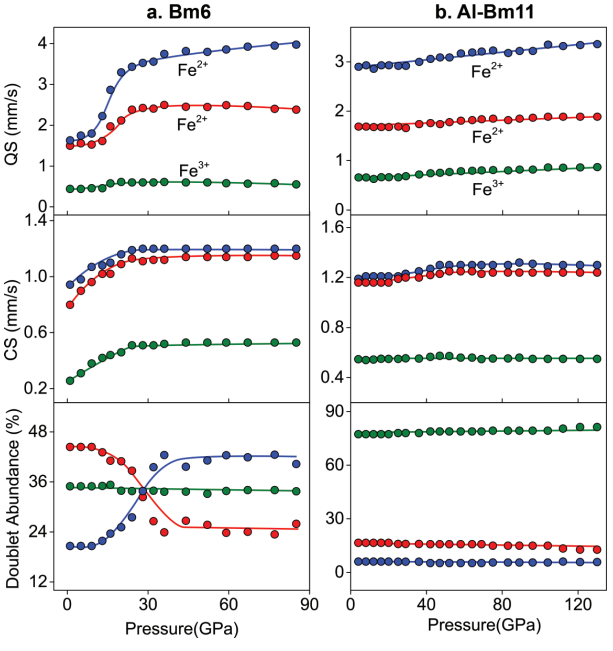

FIGURE 3. Derived quadrupole splitting (QS), chemical shift (CS), and relative doublet abundance of Fe in Bm6 and Al-Bm11 at high pressures, respectively. (**a**) Bm6; (**b**) Al-Bm11. Doublets 1 and 2 are assigned to be Fe^{2+}, while doublet 3 is assigned to be Fe^{3+}. Solid lines are shown for readers to follow the trend with increasing pressure. (Color online.)

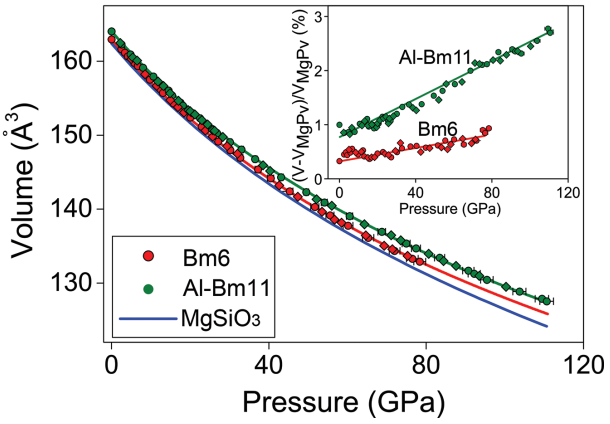

FIGURE 4. Pressure-volume relationships of bridgmanite at 300 K. Red = Bm6; green circles = Al-Bm11; blue line = $MgSiO_3$ (Boffa Ballaran et al. 2012); circles = data from the first run; diamonds = data from the second run. Corresponding lines represent the fits using the third-order Birch-Murnaghan equation to the experimental results. Inserted figure shows the variation of the unit-cell volume of Bm6 and Al-Bm11, respectively, using Mg-Bm as the reference. Uncertainties are smaller than symbols when not shown. (Color online.)

Al-Bm11 exhibit a continuous decrease with increasing pressure (Fig. 4 and Supplemental[1] Table S2). Comparison of the obtained *P-V* relationships of Bm6 and Al-Bm11 to single-crystal Mg-Bm data shows no abrupt variation in the unit-cell volume as a function of pressure. The *P-V* data for each given sample were fitted to the third-order Birch-Murnaghan EoS (Fig. 4). For Bm6, we fixed V_0 = 162.96(±0.01) Å^3 as determined by XRD measurements at ambient conditions and K'_{0T} = 4, yielding K_{0T} = 255(±2) GPa. For Al-Bm11, K_{0T} was determined to be 264(±2) GPa with K'_{0T} = 4 (fixed) and V_0 = 164.05(±0.01) Å^3 (fixed). We also constructed the confidence ellipses to demonstrate the trade-off between the derived K_{0T} and K'_{0T} for Bm6 and Al-Bm11 without fixing the K'_{0T} value (Fig. 5).

DISCUSSION

Hyperfine parameters, spin states, and lattice of bridgmanite

As shown in our Mössbauer results, QS and CS of both doublets 1 and 2, assigned to be the A-site Fe^{2+} at ambient conditions, exhibit an abrupt increase between 13 and 32 GPa, and QS of doublet 1 in Bm6 has an extremely high value of 3.5–4.0 mm/s between 32 and 85 GPa (Fig. 3 and Supplemental[1] Table S1). The observed dramatic increase in QS and the occurrence of the extremely high QS component in Fe-bearing bridgmanite are consistent with previous experimental results using both SMS and conventional Mössbauer spectroscopy (Jackson et al. 2005; Li et al. 2006, 2012; McCammon et al. 2010, 2013, 2008; Narygina et al. 2010; Potapkin et al. 2013). Some previous studies interpreted the appearance of the new extremely high-QS component as the HS to IS spin transition of Fe^{2+} in the A site (Table 1) (McCammon et al. 2010, 2013, 2008; Narygina et al. 2010; Potapkin et al. 2013). One of the main experimental supports for the presence of the IS state in the A-site Fe^{2+} is based on the observation of a partial collapse of the *K*β satellite peak and a decrease in the derived spin moment in high-pressure X-ray emission spectroscopy (XES) measurements (Badro et al. 2004; Kupenko et al. 2014; Li et al. 2004; Mao et al. 2011; McCammon et al. 2008, 2010, 2013; Narygina et al. 2010; Potapkin et al. 2013). However, the partial collapse of the *K*β satellite peak at high pressures could be interpreted as an artifact of the pressure-induced broadening of the XES spectra under non-hydrostatic conditions in the cold-compressed samples (Lin et al. 2016; Mao et al. 2014). Recent high-pressure synchrotron XES and SMS measurements on Fe-bearing bridgmanite with 38% Fe, showed the presence of an extremely high QS Fe^{2+} component (4.15 mm/s) at 126 GPa together with a partial collapse in the *K*β satellite peak (Dorfman et al. 2015). However, the spin moment for Fe-bearing bridgmanite with 38% Fe is approximately constant with increasing pressure once the pressure-induced broadening effect is corrected using the integrated relative difference method (Dorfman et al. 2015). These indicate that the occurrence of the extremely high QS Fe^{2+} component is not a result of HS to IS spin transition in bridgmanite at lower-mantle pressures (Dorfman et al. 2015; Mao et al. 2014). Importantly, a combined XES and SMS study on (Fe,Al)-bearing bridgmanite with a composition of relevance to the lower mantle showed that both Fe^{2+} and Fe^{3+} predominantly occupy the A site of the crystal lattice and remain in the high-spin state at lower mantle conditions (Lin et al. 2016).

Furthermore, theoretical studies suggest that the QS value of IS Fe^{2+} should be between 0.8 and 1.6 mm/s at lower-mantle pressures (Bengtson et al. 2009; Hsu et al. 2010), which is much lower than the QS values observed for both doublets 1 and 2 in Bm6 and results in previous Mössbauer studies (Lin et al. 2012; McCammon et al. 2008, 2010, 2013; Narygina et al. 2010; Potapkin et al. 2013). Furthermore, the IS Fe^{2+} in the A site is theoretically predicted to be not energetically favorable (Bengtson et al. 2009; Hsu et al. 2010; Hsu and Wentzcovitch 2014). A dramatic increase in the QS value of the A-site Fe^{2+} in bridgmanite should be associated with the enhanced lattice distortion but not a change in the spin state (Bengtson et al. 2009; Hsu et al. 2010; Hsu and Wentzcovitch 2014). In addition, QS of both doublets 1 and 2 in Al-Bm11 that were assigned to be the

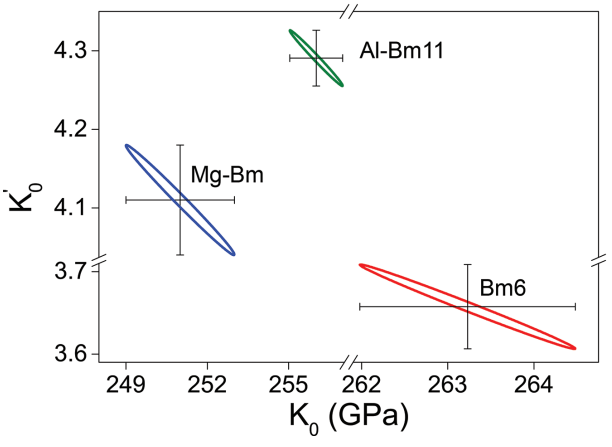

FIGURE 5. Error ellipses of K_{0T}-K'_{0T} for Bm6 and Al-Bm11 at the 1σ level. Red = Bm6; green = Al-Bm11; blue = Mg-Bm (Boffa Ballaran et al. 2012). (Color online.)

TABLE 1. Mössbauer spectroscopy results of bridgmanite at high pressures

Composition	Sample	*P* (GPa)	Valence state	Spin state	QS (mm/s)	Reference
			Fe-bearing			
$(Mg_{0.94}Fe_{0.06})SiO_3$	Single crystal	0–85	Fe^{2+}	HS	1.6–4.0	This study
			Fe^{2+}	HS	1.5–2.4	
			Fe^{3+}	HS	0.4–0.5	
$(Mg_{0.9}Fe_{0.1})SiO_3$	Powder	42–75	Fe^{2+}	HS	3.37–3.39	Jackson et al. (2005)
			Fe^{2+}	HS	2.74–2.79	
			Fe^{3+}		1.15–1.47	
$(Mg_{0.95}Fe_{0.05})SiO_3$	Powder	0–120	Fe^{2+}	HS	1.89–3.51	Jackson et al. (2005)
			Fe^{2+}	HS	1.59–2.75	
			Fe^{3+}		0.57–1.63	
$(Mg_{0.88}Fe_{0.12})SiO_3$	Powder	0–120	Fe^{2+}	HS	1.8–3.5	McCammon et al. (2008)
			Fe^{2+}	IS	3.2–4.1	
			Fe^{3+}	HS	0.6–1.5	
$(Mg_{0.6}Fe_{0.4})SiO_3$	Powder	110	Fe^{2+}	IS	4.18	Lin et al. (2008)
			Fe^{2+}	IS	3.98	
$(Mg_{0.82}Fe_{0.18})SiO_3$	Powder	120–130	Fe^{2+}	IS	4.4	McCammon et al. (2010)
			Fe^{2+}	LS	0–0.7	
$MgSiO_3$+10 mol% Fe_2O_3	Powder	40–136	Fe^{3+}	HS	0.5–1	Catalli et al. (2010)
			Fe^{3+}	LS	2.8–3.6	
$(Mg_{0.88}Fe_{0.12})SiO_3$	Powder	30–80	Fe^{2+}	IS	3.9–4.2	Narygina et al. (2010)
			Fe^{2+}	HS	2–2.7	
			Fe^{3+}	HS	0.5–1.5	
$(Mg_{0.75}Fe_{0.25})SiO_3$	Powder	135	Fe^{2+}	IS	4.1	Mao et al. (2011)
			Fe^{3+}	LS	2.99	
			Fe^{3+}	LS	1.84	
$(Mg_{0.9}Fe_{0.1})SiO_3$	Powder	0–120	Fe^{2+}	HS	1.82–4.1	Lin et al. (2012)
			Fe^{2+}	HS	1.54–3.1	
			Fe^{3+}	HS	0.65–2	
$(Mg_{0.61}Fe_{0.38}Ca_{0.01})SiO_3$	Powder	126	Fe^{2+}	HS	4.18	Dorfman et al. (2015)
			Fe^{2+}	HS	3.15	
			(Fe,Al)-bearing			
$Mg_{0.90}Fe_{0.12}Al_{0.11}Si_{0.90}O_3$	Single crystal	4–130	Fe^{2+}	HS	2.9–3.4	This study
			Fe^{2+}	HS	1.7–1.9	
			Fe^{3+}	HS	0.7–0.9	
$(Mg_{0.88}Fe_{0.09})(Si_{0.94}Al_{0.10})O_3$	Powder	12–100	Fe^{2+}		2.4–3.45	Li et al. (2006)
			Fe^{2+}		2.11–2.75	
			Fe^{3+}		0.54–0.74	
$Mg_{0.88}Fe_{0.13}Al_{0.11}Si_{0.88}O_3$	Powder	25–95	Fe^{3+}	LS	3–3.8	Catalli et al. (2011)
			Fe^{3+}	LS	2.1–2.3	
			Fe^{3+}	HS	0.6–1.3	

HS Fe^{2+} at ambient conditions only shows a weak increase with pressure (Fig. 3). In particular, QS of doublet 1 in Al-Bm11 is as high as 3–3.3 mm/s at lower mantle pressures. A recent high pressure-temperature XES study using the same Al-Bm11 sample has shown that the spin moment of Al-Bm11 is approximately constant with increasing pressure, indicating no change in the spin state of Fe^{2+} in Al-Bm11 at lower-mantle pressures (Lin et al. 2016). Together with recent theoretical results, we thus conclude that the A-site Fe^{2+} in both Fe-bearing and (Fe,Al)-bearing bridgmanite should remain in the HS state at lower-mantle pressures, and the HS to IS crossover of the A-site Fe^{2+} will not occur in bridgmanite (Bengtson et al. 2009; Hsu et al. 2010; Hsu and Wentzcovitch 2014; Lin et al. 2016).

As shown in the Mössbauer analysis, both of our Bm6 and Al-Bm11 contain a certain amount of Fe^{3+} (Fig. 3). The QS value of Fe^{3+} in Bm6 and Al-Bm11 weakly increases with pressure and is less than 1 mm/s up to 130 GPa, which is significantly lower than that of the LS Fe^{3+} in bridgmanite (Fig. 3 and Supplemental[1] Table S1) (Catalli et al. 2010, 2011; Hsu et al. 2011; Lin et al. 2012, 2013, 2016; Mao et al. 2011). This indicates that Fe^{3+} should reside in the A site in both Bm6 and Al-Bm11 crystals and stay in the HS state at lower-mantle pressures. Since our Bm6 contains minor amount of Al, the A-site Fe^{3+} should be incorporated by the coupled substitution of Al^{3+} with Mg^{2+} and Si^{4+} as well as the Mg vacancies, yielding a charge balance considering the uncertainties of the measurements (Boffa Ballaran et al. 2012; Frost and Langenhorst 2002; Hummer and Fei 2012; Lauterbach et al. 2000; McCammon 1997; Potapkin et al. 2013). In Al-Bm11, Fe^{3+} is incorporated by the coupled substitution of Al^{3+} to replace Mg^{2+} and Si^{4+} (Boffa Ballaran et al. 2012; Frost and Langenhorst 2002; Irifune et al. 1996; Lauterbach et al. 2000; McCammon 1997; Potapkin et al. 2013).

Combining the SMS with XRD results, we then investigated how the dramatic increase in the QS value and the presence of the extremely high QS component of the A-site Fe^{2+} would be associated with the EoS and lattice parameters of lower-mantle bridgmanite. Comparison of the obtained *P-V* relations of our single-crystal Bm6 to Mg-Bm shows that the unit-cell volume of Bm6 decreases continuously with pressure and does not exhibit any anomalous change (Fig. 4), indicating that the dramatic increase in the QS value of Fe^{2+} between 13 and 32 GPa does not affect the bulk unit-cell volume of bridgmanite at lower-mantle pressures. This is also consistent with recent theoretical predictions (Shukla et al. 2015). Recent studies have reported a decrease in the unit-cell volume of bridgmanite and an increase in the bulk modulus after a volume collapse that was proposed to be associated with the spin transition of B-site Fe^{3+} and/or the enhanced lattice distortion of A-site Fe^{2+} at high pressures (Hsu et al. 2011; Mao et al. 2011, 2015). The observed abnormal changes in the *P-V* data and the bulk modulus in previous studies should

only be caused by the spin transition of the B-site Fe^{3+} (Hsu et al. 2011; Mao et al. 2011, 2015; Tsuchiya and Wang 2013).

We have further evaluated the diffraction results using previously reported models (Fig. 6) (O'Keeffe and Hyde 1977). Here, the unit-cell volume of a centro-symmetrically distorted ABX_3 in perovskite structure (space group *Pbnm*, Z = 4), such as bridgmanite, can be described as follows (O'Keeffe and Hyde 1977; Zhao et al. 1993):

$$V = a \cdot b \cdot c = 32\left[B - X\right]^3 \cos^2 \Phi \quad (1)$$

where [*B*–*X*] is the bond length of the octahedra, and Φ is the titling angle of the pseudo-threefold axis of the octahedra. Although [*B*–*X*] and Φ were calculated for the octahedra in bridgmanite, the variation in the bond length and titling angle of the octahedra is expected to affect the related properties of the large dodecahedra. [*B*–*X*] and Φ of perovskite in orthorhombic structures can be approximated from the lattice parameters (O'Keeffe and Hyde 1977; Zhao et al. 1993):

$$\left[B - X\right] = b \cdot c / (4a)$$

$$\phi = \cos^{-1}\left(\sqrt{2}a^2 / bc\right). \quad (2)$$

For Bm6, [*B*–*X*] decreases linearly with increasing pressure, but the slope of [*B*–*X*] changes around 40 GPa (Fig. 6). Φ of Bm6 exhibits an anomalous softening around 40 GPa. In contrast to Bm6, [*B*–*X*] and Φ of Al-Bm11 vary continuously with pressure. Comparison of the calculated [*B*–*X*] and Φ of Bm6 to those of Al-Bm11 shows that the anomalous change in [*B*–*X*] and Φ with pressure should be associated with the dramatic increase in the QS value of Fe^{2+} in the A site with the enhanced Jahn-Teller effect, which has been observed in Bm6 but is absent in Al-Bm11 based on the SMS results (Fig. 6). It is also interesting to note that the observed anomalous change in [*B*–*X*] and Φ of Bm6 with pressure shown in the XRD data occurs at a higher pressure than that from the SMS results (Fig. 6).

We have also calculated [*B*–*X*] and Φ of the single-crystal *P*-*V* data reported by Boffa Ballaran et al. (2012) to compare with our results (Fig. 6). Both [*B*–*X*] and Φ of Fe-bearing bridgmanite (Bm4) in Boffa Ballaran et al. (2012) show a similar abnormal change with pressure as our Bm6, whereas [*B*–*X*] and Φ of (Fe,Al)-bridgmanite ($Mg_{0.60}Fe_{0.41}Al_{0.36}Si_{0.62}O_3$, Al-Bm41) in Boffa Ballaran et al. (2012) follow a similar trend with pressure as those of our Al-Bm11. Although the spin and valence states of Fe in bridgmanite were not determined in Boffa Ballaran et al. (2012), the enhanced lattice distortion of Fe^{2+} should also occur in Bm4 of Boffa Ballaran et al. (2012) but is absent in their Al-Bm41. The difference in the calculated [*B*–*X*] and Φ between Bm4 in Boffa Ballaran et al. (2012) and Bm6 in this study could be caused by the difference in the Fe^{2+} and Fe^{3+} as well as Al contents of the synthesized crystals, leading to their different axial compression behaviors (Supplemental[1] Fig. S3).

The spontaneous shear strain, e_4, of bridgmanite at lower-mantle pressures has also been evaluated from our high-pressure XRD data (Fig. 6). e_4 has been used to describe the structural change of minerals in the perovskite structure that relates the M_3^+ and R_4^+ tilting with the Jahn-Teller distortions using the complete Landau expansion (e.g., Carpenter et al. 2001; Fujishita et al. 2010; Ozaki et al. 2011; Tange et al. 2012; Wang et al. 2015). The M_3^+ and R_4^+ distortion are associated with the tilt of octahedra around the *b* and *a* axis of the orthorhombic unit cell, respectively. Analysis of the derived e_4 of Al-Bm11 shows a continuous increase with pressure, consistent with previous results for single-crystal Mg-Bm and Al-Bm41 in Boffa Ballaran et al. (2012). A softening in e_4 of our Bm6 occurs between 30 and 50 GPa, which should be related to the enhanced lattice distortion of Fe^{2+} in the A site. Similar softening in e_4 has also been identified in Bm4 in Boffa Ballaran et al. (2012), although the reduction in e_4 of Bm4 between 40 and 50 GPa is much less

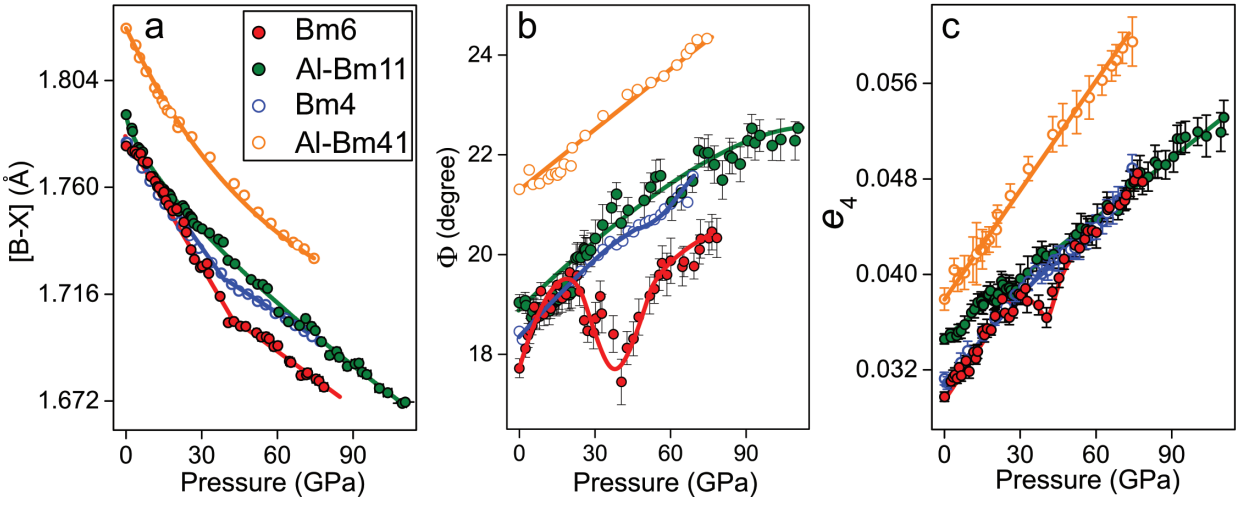

FIGURE 6. Octahedral bond length ([*B*–*X*]), octahedral tilting angles (Φ), and shear strain component (e_4) of bridgmanite at high pressures and 300 K. (**a**) Octahedral bond length, [*B*–*X*]; (**b**) Octahedral tilting angles, Φ. (**c**) Shear strain component, e_4. Red solid circles and line = Bm6; green solid circles and line = Al-Bm11; blue open circles and line = Bm4 (Boffa Ballaran et al. 2012); orange open circles and line = Al-Bm41 (Boffa Ballaran et al. 2012). Solid lines are shown for readers to follow the trend with increasing pressure. (Color online.)

than that observed in our Bm6. The sudden change in the QS of Bm6 from the SMS measurements occurs at a lower pressure than the structural change shown in XRD results, which could be a result of using different pressure media and calibrants. In addition, we have also calculated [*B*–*X*], Φ, and e_4 of bridgmanite at high pressures using literature data from polycrystalline samples (Supplemental[1] Figs. S4 and S5) (Andrault et al. 2001; Catalli et al. 2010, 2011; Dorfman et al. 2013; Lundin et al. 2008; Mao et al. 1991; Nishio-Hamane et al. 2008). These parameters are much more scattered than those from single-crystal measurements, likely due to low-resolution XRD data. Any potential anomalous change in [*B*–*X*], Φ, and e_4 thus cannot be identified from the polycrystalline data.

Combining our high-pressure SMS and XRD results and recent XES analysis (Dorfman et al. 2015; Lin et al. 2016), we conclude that both A-site Fe^{2+} and Fe^{3+} remain in the HS state at lower-mantle pressures. The presence of the extremely high QS component of the A-site Fe^{2+} in Fe-bearing bridgmanite can be explained as a result of the enhanced lattice distortion (Figs. 3 and 6) (Bengtson et al. 2009; Hsu et al. 2010; Hsu and Wentzcovitch 2014). The presence of the extremely high QS component of Fe^{2+} in Fe-bearing bridgmanite is associated with the conversion between the low QS component to the high QS component because of the crossover of the enthalpy between these two components. Theoretical calculations showed that these components of the HS Fe^{2+} have different energies, bond lengths, lattice parameters, *d*-orbital occupancies, and QS values (Bengtson et al. 2009; Hsu et al. 2014). The conversion between doublet 2 to doublet 1 in our study can be correlated with changes in the bond length and tilting angle of the octahedra and the spontaneous shear strain. In contrast, the conversion from the lower QS component to the higher QS component is not shown in Al-Bm11 (Fig. 3). Previous experimental studies have shown that addition of Al in bridgmanite can cause an apparent increase in its volume (Andrault et al. 2001; Boffa Ballaran et al. 2012). The presence of Al may decrease the difference in volume between the iron site with a high QS and the doublet 2 site with a low QS. As a result, the enthalpy of the high-QS component in our Al-Bm11 could be smaller than that of the low-QS component throughout the whole lower-mantle pressure range. This helps explain why the conversion from the low-QS doublet 2 to the high-QS doublet 1 does not occur in Al-Bm11.

Effect of Fe and Al on the EoS parameters of bridgmanite

Using our XRD results together with literature data, we have further investigated the effect of Fe and Al on the density, bulk modulus, and bulk sound velocity of bridgmanite (Figs. 7 and 8) (Andrault et al. 2001; Boffa Ballaran et al. 2012; Catalli et al. 2011; Lundin et al. 2008; Mao et al. 1991; Nishio-Hamane et al. 2008). We focus our discussion on the Fe-diluted bridgmanite with up to 15% Al because the Fe and Al content in the crystal is believed to be ~10% in the lower mantle (Irifune et al. 2010). The obtained ρ_0 and K_{0T} of our Bm6 and Al-Bm11 were first compared to the literature values of bridgmanite that did not display apparent abnormal changes in the *P*-*V* relationships (Andrault et al. 2001; Boffa Ballaran et al. 2012; Catalli et al. 2011, 2010; Lundin et al. 2008; Mao et al. 1991).

The ρ_0 of Fe-bearing bridgmanite, which is calculated from XRD measurements and electron microprobe analysis, exhibits a linear increase with its Fe content (Fig. 7) (Andrault et al. 2001; Boffa Ballaran et al. 2012; Catalli et al. 2010; Dorfman et al. 2013; Lundin et al. 2008; Mao et al. 1991, 2015). Comparing ρ_0 of our single-crystal Al-Bm11 to that of the corresponding Fe-bearing bridgmanite with the same amount of Fe shows that the presence of Al produces a decrease in the density of bridgmanite (Fig. 7). However, previous studies have shown a greater reduction in ρ_0 by the presence of Al in bridgmanite using Fe-bearing bridgmanite with the same amount of Fe as the reference (Andrault et al. 2001; Catalli et al. 2011; Nishio-Hamane and Yagi 2009; Saikia et al. 2009). It is worth noting that ρ_0 of bridgmanite in previous studies was determined from decompressed polycrystalline samples at ambient conditions (Andrault et al. 2001; Catalli et al. 2011; Nishio-Hamane and Yagi 2009). During the decompression, the powder bridgmanite sample was normally not laser-annealed to avoid the potential transformation to low-pressure phases or amorphous state. XRD peaks collected during the decompression are normally quite broad, which could result in much larger uncertainties on the derived volume and density of bridgmanite at ambient conditions. Using well-characterized and chemically homogeneous single-crystal bridgmanite samples thus allows us to provide more reliable constraints on the ρ_0.

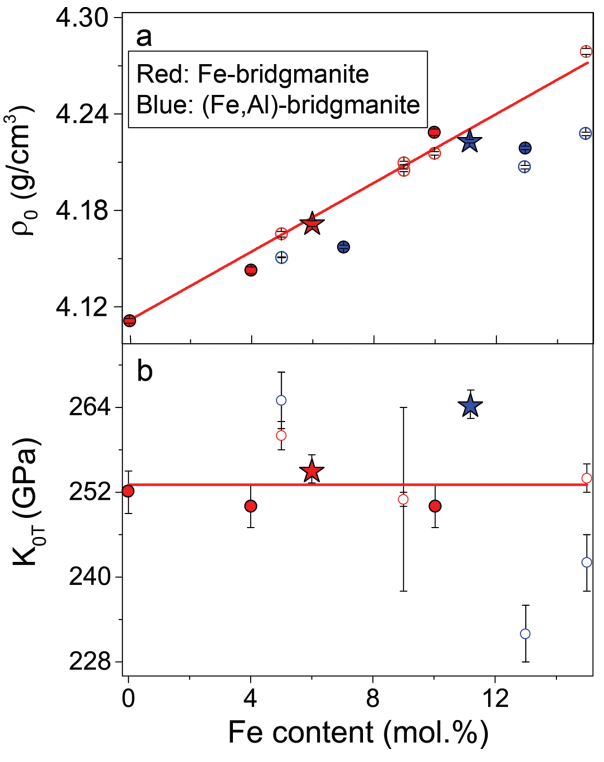

FIGURE 7. Density (ρ_0) and bulk modulus (K_{0T}) of bridgmanite at ambient conditions. (**a**). ρ_0; (**b**). K_{0T}. Red = Fe-bearing bridgmanite; blue = (Fe,Al)-bridgmanite; open symbols = results from polycrystalline bridgmanite samples (Andrault et al. 2001; Catalli et al. 2010, 2011; Dorfman et al. 2013; Lundin et al. 2008; Mao et al. 1991); solid symbols = results from single-crystal bridgmanite samples (this study; Boffa Ballaran et al. 2012; Saikia et al. 2009); stars = our Bm6 and Al-Bm11. Errors are smaller than symbols when not shown. (Color online.)

ρ_0 in Saikia et al. (2009) was also determined from XRD measurements and electron microprobe analysis of a single-crystal bridgmanite. The different trend in ρ_0 with increasing Fe content between Saikia et al. 2009 and this study could be caused by the presence of water. (Fe,Al)-bearing bridgmanite has been reported to accommodate up to 1 wt% water as structurally bond hydroxyl (Inoue et al. 2012). Synthesis of bridgmanite crystals in hydrous conditions using melt as a flux can help to grow larger crystals (Boffa Ballaran et al. 2012; Saikia et al. 2009; Okuchi et al. 2015). We note that the water content was not examined for the synthesized single crystals in Saikia et al. (2009). The presence of water can also lower the density of bridgmanite, which may help reconcile the conflicting results between our and literature results (Saikia et al. 2009).

Comparing K_{0T} of bridgmanite between different studies using literature values can be problematic due to the use of different pressure calibrants in these studies (Andrault et al. 2001; Boffa Ballaran et al. 2012; Catalli et al. 2011, 2010; Lundin et al. 2008; Mao et al. 1991). To be able to directly compare K_{0T} between different studies, we have re-calculated the experimental pressures in all previous studies without an apparent abnormal change in the *P-V* data using the internally consistent pressure scale in Fei et al. (2007) to determine the EoS parameters of bridgmanite. For studies that used Au as the pressure calibrant, pressures were re-calculated using the Au pressure scale in Fei et al. (2007), which has provided an internally consistent Pt scale used in this study (Catalli et al. 2011, 2010; Lundin et al. 2008; Mao et al. 1991). Although Andrault et al. (2001) and Boffa Ballaran et al. (2012) used ruby as the pressure calibrant, we have re-calibrated the pressures in those two studies using the Ruby pressure scale in Dewaele et al. (2004), which is most consistent with the metal pressure scales in Fei et al. (2007) and with the use of He medium in our study. We then fitted the literature *P-V* data using the third-order Birch-Murnaghan EoS with fixed K'_{0T} = 4 and fixed V_0 from XRD measurements at ambient conditions. The purpose of fixing the value of K'_{0T} is to minimize the influence of the tradeoff between K_{0T} and K'_{0T} when comparing K_0 between different studies. The error ellipses for each literature *P-V* data have been calculated to show the trade-off between K_{0T} and K'_{0T} (Fig. 8)

We found that K_{0T} of Fe-bearing bridgmanite, 253 (±3) GPa, is independent of the Fe content within experimental uncertainties (Andrault et al. 2001; Boffa Ballaran et al. 2012; Lundin et al. 2008; Mao et al. 1991) (Fig. 7). Here, our high-quality single-crystal XRD results show an increase in K_{0T} in the Fe-diluted system by the addition of Al using Fe-bearing bridgmanite as the reference. Andrault et al. (2001) also showed that the presence of Al increases K_{0T} of bridgmanite compared to the corresponding Fe-bearing phase. Yet other two studies that also used polycrystalline samples suggested a reduction of K_{0T} with Al substitution (Fig. 7 and Supplemental[1] Fig. S6) (Catalli et al. 2011; Nishio-Hamane et al. 2008). Single-crystal bridgmanite with higher Fe and Al contents also has a K_{0T} value much lower than its Fe-bearing counterpart (Supplemental[1] Fig. S6) (Boffa Ballaran et al. 2012). We note that K_{0T} of the lower-mantle ferropericlase exhibits a weak positive dependence on the Fe content, though it starts to decrease once the Fe content is greater than 20 mol% (Jacobsen et al. 2002), indicating that the enrichment of Fe may lead to a reduction in K_{0T}. Whether K_{0T} of (Fe,Al)-bearing bridgmanite exhibits a similar dependence on the Fe content to ferropericlase or not needs to be investigated in future studies using high-quality single crystals. In addition, the limited pressure of the experiments by Saikia et al. (2009), which resulted in a high K'_{0T} value of 5–6.3, may reduce the reliability of their constraints on the EoS parameters.

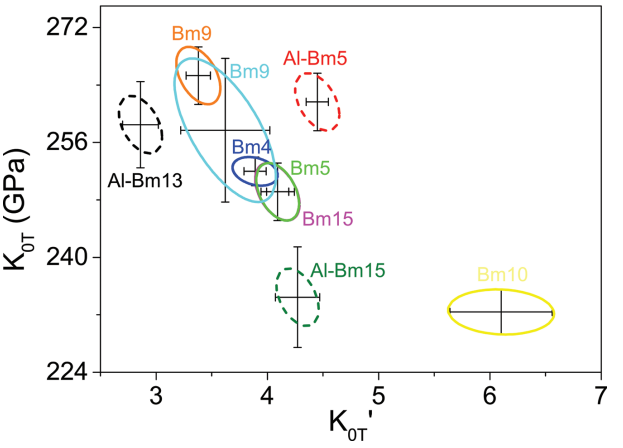

FIGURE 8. Confidence ellipses of the bulk modulus (K_{0T}) and its pressure derivative (K'_{0T}) of bridgmanite at ambient conditions at the 1σ level using literature data. Solid lines = Fe-bearing bridgmanite; dashed lines = (Fe,Al)-bridgmanite; Blue = Bm4 (Boffa Ballaran et al. 2012); green = Bm5 (Andrault et al. 2001); orange = Bm9 (Lundin et al. 2008); light blue = Bm9 (Dorfman et al. 2013); yellow: = Bm10 (Mao et al. 1991); magenta = Bm15 (Lundin et al. 2008); red = Al-Bm5 (Andrault et al. 2001); black = Al-Bm13 (Catalli et al. 2011); olive = Al-Bm15 (Nishio-Hamane et al. 2009). (Color online.)

IMPLICATIONS

Using the obtained EoS parameters, we modeled ρ and V_Φ of bridgmanite at lower-mantle pressures. The temperature effect is not included because the experimental studies on the thermal EoS parameters of bridgmanite are limited, and it is unclear how the compositional variation affects the thermal EoS parameters (Fiquet et al. 2000; Tange et al. 2012; Wolf et al. 2015). Bridgmanite in the lower mantle is expected to have an average composition of $(Mg_{0.9}Fe_{0.1})(Al_{0.1}Si_{0.9})O_3$ (Al-Bm10), which is used as the reference to understand how the enrichment of Fe and/or Al influences ρ and V_Φ. We first modeled the ρ and V_Φ profiles of bridgmanite with a composition of $(Mg_{0.8}Fe_{0.2})(Al_{0.1}Si_{0.9})O_3$ in which half of the total Fe is Fe^{2+}. Our modeling results show that $(Mg_{0.8}Fe_{0.2})(Al_{0.1}Si_{0.9})O_3$-bridgmanite has a 2.5(±0.2)% greater ρ but a 1.3(±0.7)% lower V_Φ than Al-Bm10 (Fig. 9). In this case, the enrichment of Fe in bridgmanite will exhibit a seismic signature of greater ρ but lower V_Φ. The enrichment of Al should occur with the increase in the amount of A-site Fe in bridgmanite through the coupled substitution of Al and Fe with Mg and Si. We have also calculated ρ and V_Φ of $(Mg_{0.8}Fe_{0.2})(Al_{0.2}Si_{0.8})O_3$-bridgmanite, which is enriched in both Al and Fe. We simply assumed that $(Mg_{0.8}Fe_{0.2})(Al_{0.2}Si_{0.8})O_3$-bridgmanite has a similar K_{0T} to our Al-Bm11 due to complex behavior of Fe on K_{0T} of (Fe,Al)-bearing bridgmanite. Our modeling results show

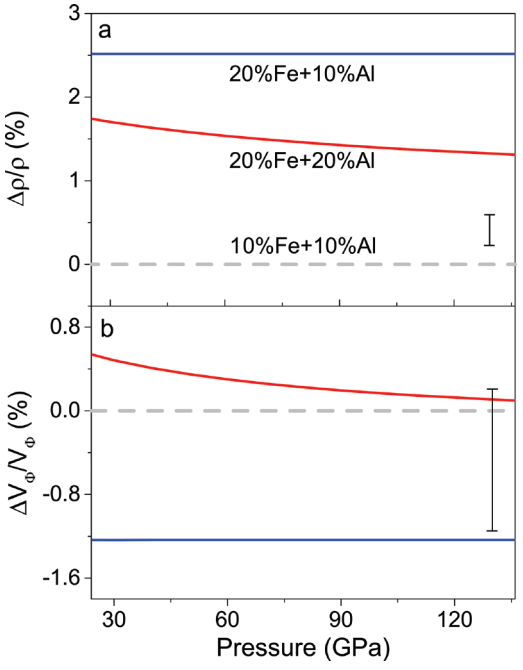

Figure 9. Variation of density ($\Delta\rho/\rho$) and bulk sound velocity ($\Delta V_\Phi/V_\Phi$) of bridgmanite at lower-mantle pressures and 300 K using Al-Bm10 as the reference. (**a**) $\Delta\rho/\rho$; (**b**) $\Delta V_\Phi/V_\Phi$. Red = $(Mg_{0.8}Fe_{0.2})(Al_{0.2}Si_{0.8})O_3$-bridgmanite; blue = $(Mg_{0.8}Fe_{0.2})(Al_{0.1}Si_{0.9})O_3$-bridgmanite; gray = $(Mg_{0.9}Fe_{0.1})(Al_{0.1}Si_{0.9})O_3$-bridgmanite. (Color online.)

that increasing the Fe and Al content in bridgmanite up to 20% [$(Mg_{0.8}Fe_{0.2})(Al_{0.1}Si_{0.9})O_3$] will lead to a $\rho \approx 1.5\%$ greater than that of Al-Bm10 in the lower mantle. Meanwhile, the combined effect of Al and Fe enrichment will produce a 0.1–0.5(±0.7)% increase in V_Φ. V_Φ of bridgmanite, which is enriched in both Al and Fe, is indistinguishable from that of Al-Bm10 considering the calculation uncertainties.

Combining our synchrotron XRD and SMS measurements on single-crystal bridgmanite and together with literature XES results (Dorfman et al. 2015; Lin et al. 2016), we conclude that A-site Fe^{2+} in Fe-bearing bridgmanite will be in the HS state in the Earth's lower mantle. For Fe-bearing bridgmanite, the enhanced lattice distortion of A-site Fe^{2+} will occur at the top of the lower mantle, resulting in an extremely high QS value of 3.5–4 mm/s. The presence of the extremely high QS Fe^{2+} component does not affect the variation of the unit-cell volume with pressure but is associated with changes in the bond length, titling angle of the octahedra, and the spontaneous shear strain. Although previous studies attributed the presence of the extremely high QS Fe^{2+} component to be a result of the HS to IS transition, which is mainly supported by the partial collapse of the *K*β satellite peak from the XES measurements, recent high-pressure and high-temperature XES studies showed that the partial collapse of the *K*β satellite peak is only an artifact of the peak broadening at high pressures (Dorfman et al. 2015; Lin et al. 2016; Mao et al. 2014). Our results support the notion that the IS state of the A-site Fe^{2+} will not occur in bridgmanite at relevant pressure and temperature conditions of the lower mantle. In (Fe,Al)-bridgmanite where Al is expected to substitute into B site, the enhanced lattice distortion of A-site Fe^{2+} is absent. Our XRD and SMS results thus provide crucial constraints on the Fe spin states, lattice, and the EoS parameters of bridgmanite at relevant pressure conditions of the lower mantle. More importantly, we further discussed the effect of compositional variation on the ρ and V_Φ profiles of the lower-mantle bridgmanite using the obtained EoS parameters. Our modeling results have shown that the enrichment of Fe will cause an enhanced ρ and a reduced V_Φ in bridgmanite, whereas the Al and Fe enrichment in bridgmanite will exhibit a seismic signature of higher ρ, but a V_Φ profile undistinguishable from bridgmanite with an average mantle composition within calculation uncertainties. These modeling results are crucial for understanding the potential chemical cause for the observed seismic anomalies in the Earth's lower mantle.

Acknowledgments

We acknowledge J. Liu for XRD measurements, C. McCammon for conventional Mössbauer measurements and data analysis, and H. Hsu for thoughtful discussion. Z. Mao acknowledges financial support from the National Natural Science Foundation of China (41522403), National Basic Research Program of China (2014CB845904), and the Fundamental Research Funds for the Central Universities in China (WK2080000052). J.F. Lin acknowledges support from the U.S. National Science Foundation (EAR-1446946). Portions of this work were performed at GeoSoilEnviroCARS, Advanced Photon Source, Argonne National Laboratory. GSECARS was supported by the National Science Foundation (EAR-0622171) and Department of Energy (DE-FG02-94ER14466) under Contract No. DE-AC02-06CH11357. Portions of this work were performed at HPCAT (Sector 16) of the Advanced Photon Source (APS), Argonne National Laboratory. HPCAT is supported by CIW, CDAC, UNLV, and LLNL through funding from DOE-NNSA, DOE-BES and NSF. A.P.S. is supported by DOE-BES, under Contract No. DE-AC02-06CH11357.

References Cited

Akahama, Y., and Kawamura, H. (2006) Pressure calibration of diamond anvil Raman gauge to 310 GPa. Journal of Applied Physics, 100, doi: 10.1063/1.2335683.

Andrault, D., Bolfan-Casanova, N., and Guignot, N. (2001) Equation of state of lower mantle (Al,Fe)-$MgSiO_3$ perovskite. Earth and Planetary Science Letters, 193, 501–508.

Badro, J., Rueff, J.P., Vanko, G., Monaco, G., Fiquet, G., and Guyot, F. (2004) Electronic transitions in perovskite: Possible nonconvecting layers in the lower mantle. Science, 305, 383–386.

Bengtson, A., Li, J., and Morgan, D. (2009) Mössbauer modeling to interpret the spin state of iron in (Mg,Fe)SiO_3 perovskite. Geophysical Research Letters, 36, doi:10.1029/2009gl038340.

Boffa Ballaran, T., Kurnosov, A., Glazyrin, K., Frost, D.J., Merlini, M., Hanfland, M., and Caracas, R. (2012) Effect of chemistry on the compressibility of silicate perovskite in the lower mantle. Earth and Planetary Science Letters, 333, 181–190.

Carpenter, M.A., Becerro, A.I., and Seifert, F. (2001) Strain analysis of phase transitions in (Ca,Sr)TiO_3 perovskites. American Mineralogist, 86, 348–363.

Catalli, K., Shim, S.H., Prakapenka, V.B., Zhao, J.Y., Sturhahn, W., Chow, P., Xiao, Y.M., Liu, H.Z., Cynn, H., and Evans, W.J. (2010) Spin state of ferric iron in $MgSiO_3$ perovskite and its effect on elastic properties. Earth and Planetary Science Letters, 289, 68–75.

Catalli, K., Shim, S.H., Dera, P., Prakapenka, V.B., Zhao, J.Y., Sturhahn, W., Chow, P., Xiao, Y.M., Cynn, H., and Evans, W.J. (2011) Effects of the Fe^{3+} spin transition on the properties of aluminous perovskite—New insights for lower-mantle seismic heterogeneities. Earth and Planetary Science Letters, 310, 293–302.

Dewaele, A., Loubeyre, P., and Mezouar, M. (2004) Equations of state of six metals above 94 GPa. Physical Review B, 70, doi:10.1103/Physrevb.70.094112.

Dorfman, S.M., Shieh, S.R., Meng, Y., Prakapenka, V.B., and Duffy, T.S. (2012) Synthesis and equation of state of perovskites in the $(Mg,Fe)_3Al_2Si_3O_{12}$ system to 172 GPa. Earth and Planetary Science Letters, 357–358, 194–202.

Dorfman, S.M., Meng, J., Prakapenka, V.B., and Duffy, T.S. (2013) Effects of Fe-enrichment on the equation of state and stability of (Mg,Fe)SiO_3 perovskite. Earth and Planetary Science Letters, 361, 249–257.

Dorfman, S.M., Badro, J., Rueff, J.P., Chow, P., Xiao, Y.M., and Gillet, P. (2015) Composition dependence of spin transition in (Mg,Fe)SiO_3 bridgmanite. American Mineralogist, 100, 2246–2253.

Dyar, M.D., Agresti, D.G., Schaefer, M.W., Grant, C.A., and Sklute, E.C. (2006) Mössbauer spectroscopy of earth and planetary materials. Annual Review of Earth and Planetary Sciences, 34, 83–125.

Fei, Y., Ricolleau, A., Frank, M., Mibe, K., Shen, G., and Prakapenka, V. (2007) Toward an interally consistent pressure scale. Proceedings of the National Academy of Sciences, 104, 9182–9186.

Fiquet, G., Dewaele, A., Andrault, D., Kunz, M., and Le Bihan, T. (2000) Thermoelastic properties and crystal structure of $MgSiO_3$ perovskite at lower mantle pressure and temperature conditions. Geophysical Research Letters, 27, 21–24.

Frost, D.J., and Langenhorst, F. (2002) The effect of Al_2O_3 on Fe-Mg partitioning between magnesiowüstite and magnesium silicate perovskite. Earth and Planetary Science Letters, 199, 227–241.

Frost, D.J., Liebske, C., Langenhorst, F., McCammon, C.A., Trønnes, R.G., and Rubie, D.C. (2004) Experimental evidence for the existence of iron-rich metal in the Earth's lower mantle. Nature, 428, 409–412.

Fujino, K., Nishio-Hamane, D., Seto, Y., Sata, N., Nagai, T., Shinmei, T., Irifune, T., Ishii, H., Hiraoka, N., Cai, Y.Q., and Tsuei, K.D. (2012) Spin transition of ferric iron in Al-bearing Mg-perovskite up to 200 GPa and its implication for the lower mantle. Earth and Planetary Science Letters, 317, 407–412.

Fujino, K., Nishio-Hamane, D., Nagai, T., Seto, Y., Kuwayama, Y., Whitaker, M., Ohfuji, H., Shinmei, T., and Irifune, T. (2014) Spin transition, substitution, and partitioning of iron in lower mantle minerals. Physics of the Earth and Planetary Interiors, 228, 186–191.

Fujishita, H., Yamada, T., Nakada, S., Okamoto, H., Shitara, S., Kato, M., and Koike, Y. (2010) Spontaneous strain in $Ba_{0.6}Ka_{0.4}BiO_3$. Physica C-Superconductivity and Its Applications, 470, S770-S771, doi:10.1016/j.physc.2009.11.023.

Glazyrin, K., Boffa Ballaran, T.B., Frost, D.J., McCammon, C., Kantor, A., Merlini, M., Hanfland, M., and Dubrovinsky, L. (2014) Magnesium silicate perovskite and effect of iron oxidation state on its bulk sound velocity at the conditions of the lower mantle. Earth and Planetary Science Letters, 393, 182–186.

Goncharov, A.F., Struzhkin, V.V., Montoya, J.A., Kharlamova, S., Kundargi, R., Siebert, J., Badro, J., Antonangeli, D., Ryerson, F.J., and Mao, W. (2010) Effect of composition, structure, and spin state on the thermal conductivity of the Earth's lower mantle. Physics of the Earth and Planetary Interiors, 180, 148–153.

Hemley, R.J., and Cohen, R.E. (1992) Silicate perovskite. Annual Review of Earth and Planetary Sciences, 20, 553–600.

Hirose, K. (2002) Phase transitions in pyrolitic mantle around 670-km depth: Implications for upwelling of plumes from the lower mantle. Journal of Geophysical Research-Solid Earth, 107, doi:10.1029/2001jb000597.

Hsu, H., and Wentzcovitch, R.M. (2014) First-principles study of intermediate-spin ferrous iron in the Earth's lower mantle. Physical Review B, 90, doi:10.1103/Physrevb.90.195205.

Hsu, H., Umemoto, K., Blaha, P., and Wentzcovitch, R.M. (2010) Spin states and hyperfine interactions of iron in $(Mg,Fe)SiO_3$ perovskite under pressure. Earth and Planetary Science Letters, 294, 19–26.

Hsu, H., Blaha, P., Cococcioni, M., and Wentzcovitch, R.M. (2011) Spin-state crossover and hyperfine interactions of ferric iron in $MgSiO_3$ perovskite. Physical Review Letters, 106, doi: 10.1103/Physrevlett.106.118501.

Hsu, H., Yu, Y.G., and Wentzcovitch, R.M. (2012) Spin crossover of iron in aluminous $MgSiO_3$ perovskite and post-perovskite. Earth and Planetary Science Letters, 359–360, 34–39.

Hummer, D.R., and Fei, Y.W. (2012) Synthesis and crystal chemistry of Fe^{3+}-bearing $(Mg,Fe^{3+})(Si,Fe^{3+})O_3$ perovskite. American Mineralogist, 97, 1915–1921.

Inoue, T., Yabuki, T., and Yurimoto, H. (2012) Water contents of Al-bearing minerals in the mantle transition zone and the lower mantle. In T. Okuchi, Ed., Joint Symposium of Misasa-2012 and Geofluid-2, p. P21–02. ISEI, Misasa, Tottori, Japan.

Irifune, T., Koizumi, T., and Ando, J-I. (1996) An experimental study of the garnet-perovskite transformation in the system $MgSiO_3$-$Mg_3Al_2Si_3O_{12}$. Physics of the Earth and Planetary Interiors, 96, 147–157.

Irifune, T., Shinmei, T., McCammon, C.A., Miyajima, N., Rubie, D.C., and Frost, D.J. (2010) Iron partitioning and density changes of pyrolite in Earth's lower mantle. Science, 327, 193–195.

Jackson, J.M., Sturhahn, W., Shen, G.Y., Zhao, J.Y., Hu, M.Y., Errandonea, D., Bass, J.D., and Fei, Y.W. (2005) A synchrotron Mössbauer spectroscopy study of $(Mg,Fe)SiO_3$ perovskite up to 120 GPa. American Mineralogist, 90, 199–205.

Jacobsen, S.D., Reichmann, H-J., Spetzler, H.A., Mackwell, S.J., Smyth, J.R., Angel, R.J., and McCammon, C.A. (2002) Structure and elasticity of single-crystal (Mg,Fe)O and a new method of generating shear waves for gigahertz ultrasonic interferometry. Journal of Geophysical Research, 107, doi:10.1029/2001JB000490.

Kupenko, I., McCammon, C., Sinmyo, R., Prescher, C., Chumakov, A.I., Kantor, A., Ruffer, R., and Dubrovinsky, L. (2014) Electronic spin state of Fe,Al-containing $MgSiO_3$ perovskite at lower mantle conditions. Lithos, 189, 167–172, doi: 10.1016/j.lithos.2013.10.022.

Lauterbach, S., McCammon, C.A., van Aken, P., Langenhorst, F., and Seifert, F. (2000) Mössbauer and ELNES spectroscopy of $(Mg,Fe)(Si,Al)O_3$ perovskite: a highly oxidised component of the lower mantle. Contributions to Mineralogy and Petrology, 138, 17–26.

Li, J., Struzhkin, V.V., Mao, H.K., Shu, J.F., Hemley, R.J., Fei, Y.W., Mysen, B., Dera, P., Prakapenka, V., and Shen, G.Y. (2004) Electronic spin state of iron in lower mantle perovskite. Proceedings of the National Academy of Sciences, 101, 14,027–14,030.

Li, J., Sturhahn, W., Jackson, J.M., Struzhkin, V.V., Lin, J.F., Zhao, J., Mao, H.K., and Shen, G. (2006) Pressure effect on the electronic structure of iron in $(Mg,Fe)(Si,Al)O_3$ perovskite: a combined synchrotron Mössbauer and X-ray emission spectroscopy study up to 100 GPa. Physics and Chemistry of Minerals, 33, 575–585.

Lin, J.F., Watson, H., Vanko, G., Alp, E.E., Prakapenka, V.B., Dera, P., Struzhkin, V.V., Kubo, A., Zhao, J.Y., McCammon, C., and Evans, W.J. (2008) Intermediate-spin ferrous iron in lowermost mantle post-perovskite and perovskite. Nature Geoscience, 1, 688–691.

Lin, J.F., Alp, E.E., Mao, Z., Inoue, T., McCammon, C., Xia, Y.M., Chow, P., and Zhao, J.Y. (2012) Electronic spin states of ferric and ferrous iron in the lower-mantle silicate perovskite. American Mineralogist, 97, 592–597.

Lin, J.F., Speziale, S., Mao, Z., and Marquardt, H. (2013) Effects of the electronic spin transitions of iron in lower-mantle minerals: implications to deep-mantle geophysics and geochemistry. Review in Geophysics, 51, 2012RG000414.

Lin, J.F., Mao, Z., Yang, J., Liu, J., Xiao, Y., Chow, P., and Okuchi, T. (2016) High-spin Fe^{2+} and Fe^{3+} in single-crystal aluminous bridgmanite in the lower mantle. Geophysical Research Letters, 43, doi:10.1002/2016GL069836.

Lundin, S., Catalli, K., Santillan, J., Shim, S.H., Prakapenka, V.B., Kunz, M., and Meng, Y. (2008) Effect of Fe on the equation of state of mantle silicate perovskite over 1 Mbar. Physics of the Earth and Planetary Interiors, 168, 97–102.

Mao, H.K., Xu, J., and Bell, P.M. (1986) Calibration of the ruby pressure gauge to 800-Kbar under quasi-hydrostatic conditions. Journal of Geophysical Research-Solid Earth and Planets, 91, 4673–4676.

Mao, H.K., Hemley, R.J., Fei, Y.W., Shu, J.F. Chen, J.C., Jephcoat, A.P., Wu, Y., and Bassett, W.A. (1991) Effect of pressure, temperature, and composition on lattice parameters and density of $(Fe,Mg)SiO_3$-perovskites to 30 GPa. Journal of Geophysical Research, 96, 8069–8097.

Mao, Z., Lin, J.F., Scott, H.P., Watson, H.C., Prakapenka, V.B., Xiao, Y., Chow, P., and McCammon, C. (2011) Iron-rich perovskite in the Earth's lower mantle. Earth and Planetary Science Letters, 309, 179–184.

Mao, Z., Lin, J.F., Yang, J., Wu, J., Watson, H.C., Xiao, Y., Chow, P., and Zhao, J. (2014) Spin and valence states of iron in Al-bearing silicate glass at high pressures studied by synchrotron Mössbauer and X-ray emission spectroscopy. American Mineralogist, 99, 415–423.

Mao, Z., Lin, J.F., Yang, J., Inoue, T., and Prakapenka, V.B. (2015) Effects of the Fe^{3+} spin transition on the equation of state of bridgmanite. Geophysical Research Letters, 42, 4335–4342, doi:10.1002/2015GL064400.

McCammon, C. (1997) Perovskite as a possible sink for ferric iron in the lower mantle. Nature, 387, 694–696.

McCammon, C., Kantor, I., Narygina, O., Rouquette, J., Ponkratz, U., Sergueev, I., Mezouar, M., Prakapenka, V., and Dubrovinsky, L. (2008) Stable intermediate-spin ferrous iron in lower-mantle perovskite. Nature Geoscience, 1, 684–687.

McCammon, C., Dubrovinsky, L., Narygina, O., Kantor, I., Wu, X., Glazyrin, K., Sergueev, I., and Chumakov, A.I. (2010) Low-spin Fe^{2+} in silicate perovskite and a possible layer at the base of the lower mantle. Physics of the Earth and Planetary Interiors, 180, 215–221.

McCammon, C., Glazyrin, K., Kantor, A., Kantor, I., Kupenko, I., Narygina, O., Potapkin, V., Prescher, C., Sinmyo, R., Chumakov, A., and others. (2013) Iron spin state in silicate perovskite at conditions of the Earth's deep interior. High Pressure Research, 33, 663–672, doi:10.1080/08957959.2013.805217.

Murakami, M., Ohishi, Y., Hirao, N., and Hirose, K. (2012) A perovskitic lower mantle inferred from high-pressure, high-temperature sound velocity data. Nature, 485, 90-U118, doi:10.1038/Nature11004.

Narygina, O.V., Kantor, I.Y., McCammon, C.A., and Dubrovinsky, L.S. (2010) Electronic state of Fe^{2+} in $(Mg,Fe)(Si,Al)O_3$ perovskite and $(Mg,Fe)SiO_3$ majorite at pressures up to 81 GPa and temperatures up to 800 K. Physics and Chemistry of Minerals, 37, 407–415.

Nishio-Hamane, D., and Yagi, T. (2009) Equations of state for postperovskite phases in the $MgSiO_3$-$FeSiO_3$-$FeAlO_3$ system. Physics of the Earth and Planetary Interiors, 175, 145–150.

Nishio-Hamane, D., Seto, Y., Fujino, K., and Nagai, T. (2008) Effect of $FeAlO_3$ incorporation into $MgSiO_3$ on the bulk modulus of perovskite. Physics of the Earth and Planetary Interiors, 166, 219–225.

O'Keeffe, M., and Hyde, B.G. (1977) Some structures topologically related to cubic perovskite ($E2_1$), ReO_3 ($D0_9$) and Cu_3Au ($L1_2$). Acta Crystallographica, B33, 3802–3813.

Okuchi, T., Purevjav, N., Tomioka, N., Lin, J.F., Kuribayashi, T., Schoneveld, L., Hwang, H., Sakamoto, N., Kawasaki, N., and Yurimoto, H. (2015) Synthesis of large and homogeneous single crystals of water-bearing minerals by slow cooling at deep-mantle pressures. American Mineralogist, 100, 1483–1492.

Ozaki, T., Kusunose, K., Yamaguchi, H., Kajiwara, K., and Chikaura, Y. (2011) Spontaneous strain of conductive strontium titanate $Sr_{1-x}LaxTiO_3$ measured by using X-ray topographic domain contrast. Phase Transitions, 84, 837–842.

Potapkin, V., McCammon, C., Glazyrin, K., Kantor, A., Kupenko, I., Prescher, C., Sinmyo, R., Smirnov, G.V., Chumakov, A.I., Ruffer, R., and Dubrovinsky, L. (2013) Effect of iron oxidation state on the electrical conductivity of the Earth's lower mantle. Nature Communications, 4, doi: 10.1038/Ncomms2436.

Prescher, C., McCammon, C., and Dubrovinsky, L. (2012) MossA: a program for analyzing energy-domain Mössbauer spectra from conventional and synchrotron sources. Journal of Applied Crystallography, 45, 329–331.

Ringwood, A.E. (1975) Composition and Petrology of the Earth's Mantle, 618 p. McGraw-Hill, New York.

Saikia, A., Boffa Ballaran, T.B., and Frost, D.J. (2009) The effect of Fe and Al substitution on the compressibility of $MgSiO_3$-perovskite determined through single-crystal X-ray diffraction. Physics of the Earth and Planetary Interiors, 173, 153–161.

Shukla, G., Wu, Z.Q., Hsu, H., Floris, A., Cococcioni, M., and Wentzcovitch, R.M. (2015) Thermoelasticity of Fe^{2+}-bearing bridgmanite. Geophysical Research Letters, 42, 1741–1749.

Stixrude, L., and Cohen, R.E. (1993) Stability of orthorhombic $MgSiO_3$ perovskite in the Earth's lower mantle. Nature, 364, 613–616.

Sturhahn, W. (2000) CONUSS and PHOENIX: Evaluation of nuclear resonant scattering data. Hyperfine Interactions, 125, 149–172.

Tange, Y., Kuwayama, Y., Irifune, T., Funakoshi, K., and Ohishi, Y. (2012) P-V-T equation of state of $MgSiO_3$ perovskite based on the MgO pressure scale: A comprehensive reference for mineralogy of the lower mantle. Journal of Geophysical Research, 117, doi:10.1029/2011jb008988.

Tsuchiya, T., and Wang, X. (2013) Ab initio investigation on the high-temperature thermodynamic properties of Fe^{3+}-bearing $MgSiO_3$ perovskite. Journal of Geophysical Research, 118, 83–91.

Tsuchiya, T., Tsuchiya, J., Umemoto, K., and Wentzcovitch, R.A. (2004) Phase transition in $MgSiO_3$ perovskite in the earth's lower mantle. Earth and Planetary Science Letters, 224, 241–248.

Vanpeteghem, C.B., Angle, R.J., Ross, N.L., Jacobsen, S.D., Dobson, D.P., Litasov, K.D., and Ohtani, E. (2006) Al, Fe substitution in the $MgSiO_3$ perovskite structure: A single-crystal X-ray diffraction study. Physics of the Earth and Planetary Interiors, 155, 96–103.

Wang, X.L., Tsuchiya, T., and Hase, A. (2015) Computational support for a pyrolitic lower mantle containing ferric iron. Nature Geoscience, 8, 556–559.

Wolf, A.S., Jackson, J.M., Dera, P., and Prakapenka, V.B. (2015) The thermal equation of state of $(Mg,Fe)SiO_3$ bridgmanite (perovskite) and implications for lower mantle structures. Journal of Geophysical Research-Solid Earth, 120, 7460–7489, doi:10.1002/2015JB012108.

Zhao, Y.S., Weidner, D.J., Parise, J.B., and Cox, D.E. (1993) Critical phenomena and phase transition of perovskite data for $NaMgF_3$ Perovskite. Part II. Physics of the Earth and Planetary Interiors, 76, 17–34.

Manuscript received March 16, 2016
Manuscript accepted August 29, 2016
Manuscript handled by Sergio Speziale